Heliyon 5 (2019) e01749

Contents lists available at ScienceDirect

Heliyon

journal homepage: www.heliyon.com

Aqueous extract from *Madhuca indica* bark protects cells from oxidative stress caused by electron beam radiation: *in vitro, in vivo and in silico* approach

K. Vinutha [a], Gollapalli Pavan [b], Sharath Pattar [c], N Suchetha Kumari [d], S.M. Vidya [a,*]

[a] *Department of Biotechnology, NMAM Institute of Technology, 574110, Udupi (Dist), Nitte, Karnataka, India*
[b] *Department of Biotechnology Vignan's Foundation for Science, Technology and Research (Deemed to be University), Vadlamudi, Guntur (Dt), Andhra Pradesh, 522203, India*
[c] *National Bureau of Agriculturally Important Insects, P.Bag No: 2491, H.A. Farm Post, Bellary Rd, Hebbal, Bengaluru, Karnataka, 560024, India*
[d] *University Enclave, Medical Sciences Complex, Deralakatte, Mangalore, 575018, India*

ARTICLE INFO

Keywords:
Biochemistry
Bioinformatics
Biotechnology
Computational biology
Molecular biology
System biology
Structural biology

ABSTRACT

In an endeavor to find the novel natural radioprotector to secure normal cells surrounding cancerous cell during radiation exposure, *Madhuca indica* (*M. indica*) aqueous stem bark extract was evaluated for radioprotective activity using *in vitro*, *in vivo,* and *in silico* models. *M. indica* extract exhibited concentration dependent protective effect on electron beam radiation (EBR) induced damage to pBR322 DNA; the highest protection was achieved at 150 μg concentrations. Similarly, *M. indica* extract (400 mg/kg) administrated to mice prior to irradiation protected DNA from the radiation damage, which was confirmed by inhibiting comet parameters. The study showed a significant increase in the levels of glutathione and superoxide dismutase levels. The study also revealed that administration of *M. Indica* at the different dose to mice significantly reduced EBR induced MDA, sialic acid and nitric acid levels. Further extract prevented histophatological changes of skin and liver. In contrast, protein-protein interaction studies were performed to find the hub protein, involved in radiation-induced DNA damage. Among 437 proteins that are found expressed during radiation, p53 was found to be a master protein regulating the whole pathway. Molecular interaction between p53 and *M. indica* extract was predicted by quantitative structure-activity relationship and ADMET properties. Biomolecules such as quercetin, myricetin, and 7-hydroxyflavone were found to be promising inhibitors of p53 protein and may help in the protection of EBR induced DNA damage during cancer treatment.

1. Introduction

Cancer is a leading cause of death worldwide. The disease accounted for 9.6 million deaths (around 17.09 % of all deaths worldwide) in 2018 and its associated mortality rate is expected to increase even further [WHO report, 2018]. One of the treatments for curing cancer is the use of radiation therapy, which uses ionizing radiation (IR) as a source of treatment. IR mainly causes irreparable damage to the critical targets within the cell, such as DNA and other important biomolecules (Szumiel, 2006). DNA-double stranded breaks (DSB) are the most lethal events among IR-induced DNA lesions, both numerical and structural chromosome aberrations increases if not properly repaired (Sancar et al., 2004). However, radiation therapy is considered the important method to treat cancer; there still remains a substantial toxicity for normal tissues and organs. Unfortunately, as long as toxicities is occurring in the interim of clinical therapy, higher radiation doses cannot be used for treatment which would be more effective in patients undergoing radiotherapy (Grover and Kumar, 2002). Hence, improving the therapeutic ratio and to reduce cellular toxicities, there is a need for tremendous research in search of radioprotective drugs. Also, if molecular mechanism of action of cell response during irradiation is known, it will help to develop potent radioprotector to enhance the DNA repair process and ultimately rescue cells from death.

Protein-protein interaction (PPI) studies contribute a wide range of data in predicting the function of protein and its drug interaction ability at molecular level (Hormozdiari et al., 2010). It is known that, over 85% of proteins do not function alone, rather it complexes with other proteins for its operation (Berggard et al., 2007). The consequential analysis of

* Corresponding author.
E-mail address: drvidyasm@nitte.edu.in (S.M. Vidya).

https://doi.org/10.1016/j.heliyon.2019.e01749
Received 22 November 2018; Received in revised form 18 April 2019; Accepted 13 May 2019

corroborated proteins shows that, proteins involved in the same cellular processes are frequently found to be interacting with each other (von Mering et al., 2002). Revealing the protein-protein interaction complexity helps in the identification of drug targets (Pedamallu and Posfai, 2010). Therefore, it is important to find the criteria for selecting the most probable protein-protein interactions having biological importance. Hence, the computational analysis of PPI networks is used to understand the various functions of unexplored proteins (Gavin et al., 2002). Further, molecular docking studies help to activate or inhibit the process cascade providing specific lead molecule which would act as radioprotector (Durga et al., 2010). Attempts have been made to find the potent radioprotective agent, however, the fact remains that there is nosingle radioprotective drug available which meets all the prerequisites of an ideal radioprotector i. e no toxicity, high stability and easy administration. In this concern, the search for less toxic and more potent natural radioprotective drugs continues.

M. indica is a flowering plant belongs to the family Sapotaceae, grown widely in deciduous forests of Indian states. *M. indica* is being used from centuries for numerous purposes as a medicinal herb. The bark of *M. indica* is used for treating rheumatism, ulcer, itches, bleeding, spongy gum and tonsillitis (Dahake and Chiratan, 2010). Stem bark is also reported having inhibitory activity on free radicals release from phagocyte (Pawar et al., 2004). The methanol extracts of flower and stem bark have been reported for antibacterial activity (Das and Choudhary, 2010). Based on the medicinal significance, we have evaluated the radioprotective activity of *M. indica* stem bark extract using *in vitro* and *in vivo* models and its screened constitutes using *in silico* models.

2. Materials and methods

2.1. Chemicals

TRIS base, high melting agarose, low melting agarose, disodium EDTA, tritonX-100, sodium sarcosinate, DMSO and propidium iodide for performing comet assay, Thiobarbituric acid, N-1-napthylethylenediamine dihydrochloride, sulfanilamide, sulphuric acid, sodium periodate, cyclohexanone for conducting MDA, NO and sialic acid assay were obtained from Sigma Aldrich (St.Louis, Missouri). All biological assay reagents, SGPT, SGOT, total bilirubin, ALP, albumin, total protein kits and plasmids pBR322 and HISTOPAQUE were purchased from Bangalore Genei, India.

2.2. Collection and extraction

Stem barks of *M. indica* was collected from Western Ghats region, Udupi Karnataka. The plant was identified and authenticated by the expert Taxonomist, Department of Botany, Mangalore University, India. The material was dried in shadow for 6–8 weeks and finely powdered to store for further use in air tight containers for further studies. Aqueous stem bark extract of *M. indica* was prepared by boiling bark powder in distilled water for 20 min with intermittent shaking for next two days followed by filtration to remove insoluble. The filtrate was concentrated in vacuum using a rotary evaporator at 25 °C. Solvents leftover was completely removed on a water bath, dried and used for further analysis (Akinmoladun et al., 2007).

2.3. Subchronic toxicity studies

2.3.1. Ethical approval

The study was approved by institutional animal ethics committee i.e. K. S. Hegde Medical Academy, Mangalore, India (**KSHEMA/AEC/40/2011**) by strictly adhering to its guidelines

2.3.2. Animals

Swiss albino mice weighing 22–25 g were obtained from the institutional animal breeding section, K. S. Hegde Medical Academy, Mangalore, India. They were maintained under the standard condition of temperature and humidity in the centers animal house facility. Animals were provided with a standard mouse chow and water ad libitum and the experiments were carried out with the prior approval of the institutional animal ethics committee (K. S. Hegde Medical Academy, Mangalore, India) by strictly adhering to its guidelines

2.3.3. Toxicity studies

Subchronic toxicity studies of the *M. indica* aqueous extract was carried at K. S. Hegde Medical Academy, Mangalore, India (KSHEMA/AEC/40/2011). The study was conducted using a standard kit provided by Agappe according to manufacturer's instructions. To carry out toxicity studies Swiss albino mice were divided into two groups of six animals each and were starved for 18 h prior to the experiment. Group I: Control; group II: were fed orally with *M. indica* aqueous extract suspended in distilled water at the concentration of 2000 mg/kg body weight. The treatment carried out for 30 days, food and water intake was supervised daily. The animal was sacrificed on 31st day; blood was drawn by cardiac puncture and was centrifuged at 3,500 rpm for 5mins using table centrifuge. Finally, serum was collected and used for enzyme estimation.

2.4. Irradiation

The irradiation work was conducted at Microtron centre, Mangalore University, Mangalore, Karnataka, India. The un-anaesthetized animals were restrained in well-ventilated perspex boxes and exposed to whole-body EBR at a distance of 30 cm from the beam exit point of the microtron accelerator at 6Gy radiation dose at the dose rate of ~100 Gy/min. The pBR322 plasmid DNA were exposed to EBR at 20 cm from the beam exit point of the Microtron accelerator at 4 Gy radiation dose.

2.5. In vitro DNA damage studies using pBR322 plasmid DNA

To evaluate the effect of bark extract on EB radiation induced strand breaks *in vitro*, the plasmid pBR322 (250 ng) in phosphate buffer (0.1M, pH 7.4) was exposed to EB radiation (1–8Gy) in the absence of the extracts for dose fixation [Gorbounova et al., 2000.]. After irradiation, the DNA was electrophoresed, stained with ethidium bromide and the DNA bands were photographed and quantified by using TotalGelLab quanta V. 12.2. Once radiation dosage was fixed another sets of vials containing pBR322 DNA samples were divided in to 6 sets. Set 1: control; set II: radiated control; set III, IV, V and VI were treated with *M. indica* extract at 50, 100, 150 and 200 μg/ml respectively prior to irradiation. The DNA in each vials were treated with the extracts at different concentrations viz. 50, 100, 150 and 200μg of aqueous extracts individually; on treatment they were immediately exposed to EB radiation at the dose of 4 Gy/min. After exposure, the DNA samples were electrophoresed on 1% agarose gel stained with Gold View containing TAE buffer and photographed using UV transilluminator and quantified with software TotalGelLab quanta V.12.2.

2.6. In vivo DNA damage study

2.6.1. Estimation of DNA damage

To perform *in vivo* DNA damage studies, animals were divided into five groups of six animals each as follows: group I: served as controls; group II: irradiated control; group III, IV and V were treated with 100, 200 and 400 mg/kg body weight of extract once in a day for 15 consecutive days and on 16th-day mice were exposed to 6 Gy EB radiation (Madhu et al., 2012). After irradiation, they were monitored for the next 15 days and they were sacrificed by cervical dislocation on the 16th day. The blood was drawn from mice and lymphocytes from blood was isolated and used to carry out comet assay.

2.6.2. Separation of lymphocytes

Lymphocytes were separated from whole blood using HISTOPAQUE-

1077 as method described by Denhlom (Denholm and wolber, 1991).

2.6.3. Comet assay

In order to estimate DNA damage in blood lymphocytes, 10μl lymphocyte sample was mixed with 200μl of 0.5% low melting agarose at 27 °C and layered on frosted slides pre-coated with 200μl 0.6% high melting agarose (Singh, 2000). During the polymerization of each gel-layer, the slides were kept on ice. After solidification, the cover slips were removed and were kept in pre-chilled lysing buffer (1% sodium sarcosinate, 2.5M NaCl, 100mM Na_2 EDTA, 10mM Tris-HCl, 1% Triton X-100 and DMSO 10%) for 1h. The slides were removed from the lysis solution and placed on a horizontal electrophoresis tank filled with the alkaline buffer (0.2M NaOH, 1mM Na_2EDTA, pH 10) and then equilibrated with the same buffer for 20min. Electrophoresis was carried out for 20 min at 2 V and 20 mA and neutralized with 0.4M Tris, pH 7.4, stained with 50μl of ethidium bromide and observed using fluorescence microscope (Olympus. 40x objective). The level of DNA damage was assessed from the DNA migration distance by subtracting the diameter of the nucleus from the total length of the comet. 50 randomly selected cells were examined for each replicate and for each sample. The quantification of the DNA strand breaks of the stored images was performed using CASP software (www.casplab.com) by which the percentage of DNA in the tail (%T), tail length (TL) and olive tail moment (OTM) could be obtained directly.

Simultaneously serum was collected from remaining amount of blood and used to carry sialic acid test; the liver homogenate prepared using cold normal saline was used for conducting malondialdehyde (MDA) and nitric oxide (NO) assay.

2.6.4. Estimation of reduced glutathione

Proteins were precipitated using 10% TCA, centrifuged and 0.5ml of supernatant was mixed with 0.3M phosphate buffer and 0.006mM DTNB. The mixture was incubated for 1min and the absorbance was measured at 412nm against appropriate blank. The glutathione content was calculated by using standard plot under the same experimental condition (Jindal et al., 2009).

2.6.5. Estimation of superoxide dismutase activity

Nitro blue tetrazolium chloride is used as a substrate for the assay, which reacts with superoxide anions formed upon illumination of riboflavin in the presence of methionine so has to produce blue colored complex i.e. formazan. Presence of SOD in the sample will act on the superoxide anions formed by riboflavin thereby reducing the superoxide anions in the substrate, in turn, dropping the production of formazan exhibiting a decreased intensity of blue color formation. This is directly proportional to the amount of SOD in the sample, 50% decrease in the formation of formazan is taken as one unit of SOD.

2.7. Evaluation of anti-inflammatory activity of bark extracts induced during radiation

2.7.1. Estimation of malondialdehyde

Malondialdehyde was evaluated as described by Ohkawa et al., 1979. Malondialdehyde level of samples were assayed by incubating the liver homogenate with 15% TCA, 0.275%TBA and 5N HCL at 95 °C for 15min, the mixer was cooled, centrifuged and the absorbance of the supernatant was measured at 522nm against an appropriate blank. The results were expressed as nmol/mg of protein.

2.7.2. Estimation of nitric oxide

Total nitric oxide levels were calculated by the conversion of nitrate into nitrite and it was measured by the Greiss reaction (Crow and Ischiropoulos, 1996). Briefly; 20μl of each sample was incubated with an equal volume of sulfanilamide solution (1% sulfanilamide in 5% phosphoric acid) at room temperature for 5–10min, which is protected from light. After incubation 50μl of the NED (0.1% N-1-napthylethylenediamine dihydrochloride in water) was added and incubated.

2.7.3. Estimation of sialic acid

Sialic acid was evaluated as described by Warren (Warren, 1959). 0.2 ml of serum and 0.2ml of sialic acid standard was pippeted out in separate 15 × 150mm test tubes and marked test and standard respectively. To each tube 4.8ml of 5% TCA was added with shaking, the tubes were covered with aluminum foil and placed in already boiling water bath. After exactly 15 min the test tubes were removed and immersed in cold water. The cooled sample is filtered through Whatman No. 1 filter paper. Two tubes were set up and 2ml filtrate was pippeted into each of the pair of tubes. The tubes containing filtrate from the standard were marked as standard and standard–blank respectively.

Reagent blank containing 2 ml of 5 % trichloroacetic acid was prepared and 4 ml of acetic acid mixture was pippeted into the three test tubes marked blank. 4 ml of diphenylamine reagent was pippeted into the tubes marked test and standard. All the tubes were mixed gently on a vertex mixture, covered with aluminum foil and incubated in boiling water for 20min. The test tubes were cooled in water bath and absorbance at 520nm in a suitable calorimeter or spectrophotometer set at zero with reagent blank was determined.

2.7.4. Histopathological studies

Slice of liver and skin were fixed in 5% formaldehyde then embedded in paraffin wax later sectioned at 5μ thickness and finally stained with haematoxylin and eosin stain. Detailed microscopic examination these organs were carried out.

2.8. In silico DNA damage studies

2.8.1. Construction of PPI network

Proteins expressed during irradiation were retrieved from PubMed database queries using four following keywords: irradiation, ionizing radiation, gamma radiation, and radiotherapy (Yang et al., 2009). A total set of 437 proteins was identified that have been expressed during the irradiation [Table S1]. The individual interaction partners of all the 92 proteins involved in the DDR were collected from the STRING database by using the following prediction methods: neighborhood, gene fusion, co-occurrence, experimental, databases and text mining methods [Table S2] (Suel et al., 2000). The scoring method used for interactions was divided into different confidence ranges, i.e. low confidence, medium confidence, high confidence, and highest confidence ranges if the score is < 0.2, ≤ 0.7, ≤ 0.9 and > 0.9 respectively. The cutoff score of 0.7 was set to select interactions, which are in the final network. The number of interacting partners to view the network was set to ≤ 10 interactions. Later, PPI network was constructed with the data obtained from the string database and visualized by using Cytoscape (Shannon et al., 2002). Further, the network was analyzed to detect the hub protein (node) based on the bottleneck ranking method using a Cytohubba plug-in of Cytoscape (Shu-Hwa et al., 2010).

2.8.2. Validation of network

Topological matrices have been utilized to identify the potential false positive interactions such as connectivity, the degree of distribution, clustering coefficient, shortest path, betweenness centrality and closeness centrality.

2.8.2.1. Connectivity (or) degree. The most basic characteristic of a node is its degree *d*, which represents the number of links between the nodes in the network. For directed networks, *d* has two components *d*, in and *d*,out. The 'in-degree' refers to a number of incoming edges and ' 'out-degree' refers to a number of out-going edges respectively, which adds upto *d* (Barabasi and Oltvai, 2004).

2.8.2.2. Degree of distribution. The degree of distribution (P (*d*)) gives the feasibility that a selected node has exactly *d* links. P (*d*) is mainly obtained by counting the number of nodes N (*d*) with d = 1, 2. . . links and dividing by the number of nodes N. The degree of distribution helps to distinguish between various network topologies (Watts and Strogatz, 1998).

2.8.2.3. Clustering coefficient. Clustering coefficient is a degree of measurement to which nodes in the network tend to cluster together. It is commonly employed to identify the well connected subcomponents in the network. It mainly represents the interconnectivity of the neighboring nodes. The clustering coefficient 'C' for all nodes *d* is a notion of how neighbors of a given node are connected. The node with the high clustering coefficient is said to have the high connected neighbor (Diestel, 2000). The clustering coefficient for a directed network is represented as.

$$CC\ (d) = 2nd/Kd\ (Kd-1)$$

where *nd* represents the number of triangles that go through the node *d* and Kd indicates the degree of the node. The denomination (d) refers to the maximum number of triangles that can go through the node *d*.

2.8.2.4. Shortest path. Shortest path explains about the network's diameter 'i', which is the greatest distance between any two nodes in the network (Diestel, 2000). It can also be interpreted as the length of shortest path in the network and is represented as.

$$i = \max\ iG\ (u,v)$$

where iG (*u,v*) is the shortest path between u and v node in network G.

2.8.2.5. Betweenness centrality. Betweenness centrality (BC) is the measure of node centrality in the network based on the highest connectivity. It is equal to the number of shortest paths from all vertices of the node to the rest of others that pass through that node (Freeman, 1977). A node with the highest BC has a large influence on the transfer of items through the network, under the assumption that item transfer follows the shortest paths.

$$Cb\ (v) = \sum s \neq t\ (\sigma st\ (n)/\sigma st)$$

where σst is the number of shortest paths form's' to't', and σst (v) is the number of shortest paths form's' to't' that pass through a vertex 'v'. A similar definition for 'edge betweenness' is given by (Girvan and Newman, 2002).

2.8.2.6. Closeness centrality. The closeness centrality is a measure of how fast the information spreads from a given node to the other reachable node in the network. The closeness centrality (CC) Cc (n) of a node *n* is defined as the reciprocal of the average shortest path length (Newman and Girvan, 2005) and is computed as follows.

$$CC\ (n) = 1/\text{avg}\ (L(u,v))$$

where L (*u,v*) is the length of the shortest path between two nodes *u* and *v*. The CC of each node is a number between 0 and 1.

2.9. Preparation of ligands structure

Total 25 chemical structures of *M. indica* phytoconstituents were identified and collected from the previous literature (Chakma, 2011). The 2D structures of these compounds were obtained from NCBI (http://www.ncbi.nlm.nih.gov/PubChemcompound/) in SDF format and they were converted into 3D (PDB) format using ChemDraw Ultra 6.0.

The molecular descriptors of the phytoconstituents were obtained using molinspiration server (http://www.molinspiration.com/). Molinspiration server provides information regarding the molecular weight (MW), Log P (partition coefficient) values, topological surface area (TPSA), number of H-bond donors (nOHNH), number of H-bond acceptors (nON) and number of rotatable bonds (nrotb) for the lead molecules [Table S3].

2.10. Quantitative structure activity relationship (QSAR)

Data sets of 25 compounds of *M. indica* were selected for QSAR analysis. Chemical structures and biological activity for the complete set of compounds were divided into training and test sets. The half maximal (50 %) inhibitory concentration of compounds (IC50) employed in this study (varying from 0.021 to 100 μM), were converted to the corresponding pIC50 (-logIC50) and used as dependent variables in the QSAR investigations. From the original data set of 25 compounds, 19 compounds [1 to 18, Table S3] were selected as training set and 7 compounds [19 to 25, Table S3] as test set. Discovery Studio 2.5 software (DS 2.5) was used to perform QSAR studies (Chandra, 2001).

2.10.1. Absorption, distribution, metabolism, excretion and toxicity (ADMET)

The ADME properties of *M. indica* phytoconstituents were calculated using Accelrys Discovery Studio tool in which the various pharmacokinetics parameters like blood brain barrier penetration (BBB), absorption level, solubility level, hepatotoxicity, CYP2D6, plasma protein binding (PPB) levels were estimated. Obtained results were cross checked with standard values provided by Accelrys (Rogers and Hopfinger, 1994). The toxicity profile of the compounds were predicted using TOPKAT, which uses a range of quantitative structure toxicity relationship (QSTR) models for assessing special toxicological endpoints such as aerobic biodegradability, mutagenicity, developmental toxicity prediction and skin irritation test (Gade et al., 2012).

2.11. Molecular docking studies

2.11.1. Preparation of protein structure for docking

The 2D X-ray crystal structure of p53 protein (chain C) was retrieved from the PDB (Daisy and Suveena, 2012). Before docking, all the water molecules were removed and H-atom were added to the protein file for correct ionization and tautomeric states of amino acid residues such as aspartic acid, serine, glutamine, arginine and histidine (Nair et al., 2010). Based on results obtained from the QSAR and ADMET, compounds such as betulonic acid, camelliagenina, myricetin and querciten were chosen as lead compounds for docking studies.

2.11.2. Determination of active site and molecular docking studies

The Q site finder server was used for the identification of the most potential active site of p53 protein, where the ligand can bind and interact (Sankar and Shanmughavel, 2010). The docking of the prepared ligands with p53 protein receptor was determined using Biosolve-IT FlexX; a commercial tool to identify the active potential drug.

2.12. Statistical significance

All results were expressed as mean ± standard Deviation (S.D). Statistical significance was determined using one-way analysis of variance (ANOVA). p values < 0.05 were considered as significant. All statistical analysis was carried out using Dunnett's test using an instant statistical package (Graph Pad Prism version 3.0).

3. Results and discussion

3.1. Preparation of extracts

The yield of aqueous extracts of *M. indica was* found to be 16.5 %. The extract was used for further studies.

3.2. Subchronic toxicity studies

The effect of aqueous extract *M. indica* on serum biochemical parameters presented in [Table S4]. The levels of enzymes such as SGOT, SGPT, ALP, albumin, total protein and bilirubin content were not significantly different compared to control groups. From the results it was confirmed that extracts do not show any toxicity even after administering the dose of 2000 mg/kg b. w. similar reports of toxicity evaluation were observed in the studies of Pearl Dias et al. (Pearl et al., 2014). Where in the study showed that the combination of extract in 1:1 combination of the aqueous extracts of *F. racemosa* stem bark and *M. indica* leaves at 2000 mg/kg b. w. did not show any toxic effect.

3.3. Protection of pBR322 plasmid DNA from EB radiation

The presence of aqueous extract of *M. indica* during irradiation protected pBR322 plasmid DNA from radiation induced lesions. An exposure of 4 Gy EB radiation, the plasmid DNA suffered strand breaks, which converted the super coiled (sc) form of plasmid DNA to open circular form (oc) (Fig. 1a, lane 2). However, the presence of *M. indica* stem bark extract inhibited the conversion of sc to oc forms at dose dependent manner. The reduction in sc form of DNA was found to be directly proportional to radiation dose due to the induction of strand breaks in the DNA, because DNA is considered to be critical target in cell from point of radiation damage (Vedansha et al., 2012). The highest protection was achieved at 150 μg/ml (76 %) compared to other concentrations (Fig. 1b). The result is similar to work reported by Nitin et al. (Nitin and Cherupally, 2004), who showed that treatment of diethyldithicarbamate at 100 μM concentration along with γ-irradiation at 50 Gy/min resulted in a significant protection of pBR322 DNA damage in a dose-dependent manner.

3.4. Estimation of DNA damage in vivo

3.4.1. M. indica stem bark extract inhibited the comet parameters

The results of alkaline comet assay indicated that administration of the extract of *M. indica* at different concentrations prior to irradiation protected the cellular DNA by inhibiting the comet parameters such as tail length (TL) it shows breaks in DNA and its density, olive tail moment (OTM) indicates fragmentation of DNA and percentage of DNA in tail (% T) it provides a quantitative measure of the damaged DNA when compared to control [Table S5], indicating its significant role in radio protection. One of the deleterious consequences of DNA damage from exposure to IR is the induction of cancer. Protecting cellular DNA from radiation damage will result in the prevention of the cancers induced by radiation. The comet assay is especially capable of measuring acute effects on DNA integrity at high concentrations. The result was supported by studies of Gopinathan et al.(Gopinathan and cherupally, 2013) who showed that administration of gallic acid at different dose 100, 200, 400 mg/kg b. w reduced the radiation induced (8Gy^{60} Co-γ-rays) cellular DNA damage in mouse peripheral blood lymphocytes using single cell gel electrophoresis. Here also comparably at 400 mg/kg b. w protection was more which showed concentration dependent protection.

3.4.2. Estimation of reduced glutathione

GST is an enzyme involved in the detoxification process. EBR decreased the GSH (μg/ml) activity in the liver (Fig. 2), *M. indica* treated mice significantly restored the GSH activity in a dose-dependent manner. There was a diminution in the GSH level in the radiated mice when compared to the normal mice. The cells in normal conditions will be very intact healthy and the levels of GSH is restored by synthesis. The GSH levels in irradiated mice were increased by *M. indica* and the levels are close to normal mice. Similar results were observed by (Jaetia et al., 2003). Who showed that, administration of ginger increased the GST levels in mice on exposure to 6–12 Gy gamma radiation.

3.4.3. Estimation of superoxide dismutase (SOD)

The whole body EBR decreased the SOD activity (U/mg of protein) in the liver (Fig. 3), *M. indica* dose-dependently restored the SOD activity. Exposure of mice to 6 Gy EBR resulted in significant decrease in SOD activity as compared to that in control. Oral administration of *M. indica* to mice pre exposure to EBR significantly abrogated the EBR induced reduction in SOD activity. Xiaojing et al. in his review article explains how the SOD, the unique enzyme responsible for the dismutation of superoxide radicals and is expected to occupy an indispensable position in the treatment of ROS-mediated tissue damage caused from radiation exposure. Later Kumar KB et al. (Kumar KB et al. 2004) showed that pre treatment of Phyllanthus amarus increased the activity of antioxidant

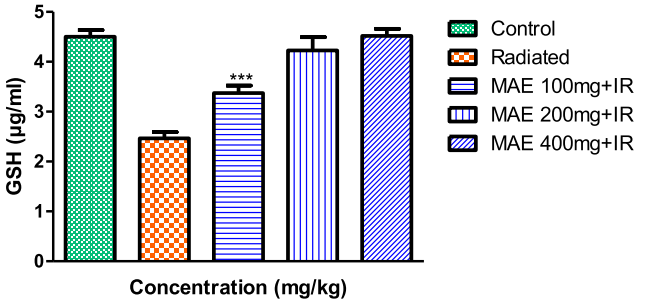

Fig. 2. Effects of *M. indica* on GSH in liver after whole body electron beam irradiation. Values are means ± SE of 6 mice in each group, **statistical significant at $p < 0.01$ and *$p < 0.05$ when compared to the radiation group.

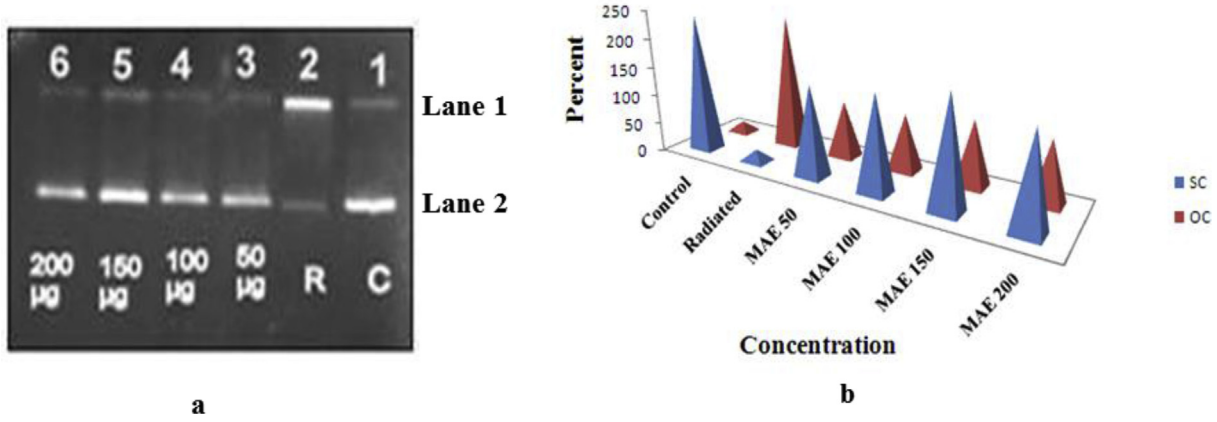

Fig. 1. Protection of pBR322 DNA with combined aqueous extracts of *M. indica* (a) and quantification of extinct of DNA damage (b). C: control, RC: radiated control; MAE: *M. indica* aqueous extract.

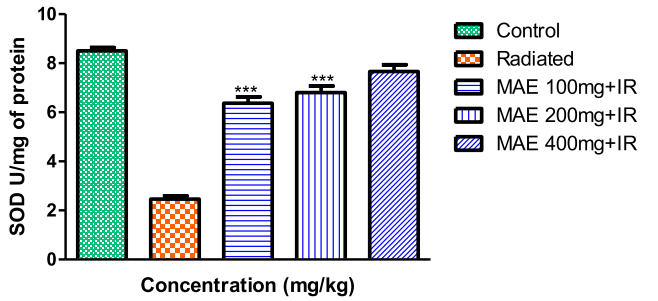

Fig. 3. Effects of *M. indica* on SOD activity in liver after whole body electron beam irradiation. Values are means ± SE of 6 mice in each group, ***statistical significant at $p < 0.001$ when compared to the radiation group.

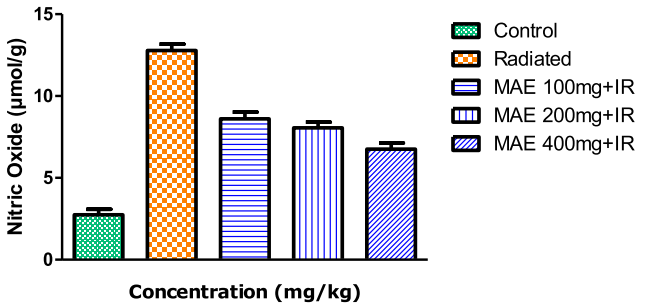

Fig. 5. Effects of *M. indica* on nitric oxide activity in liver after whole body electron beam irradiation. Values are means ± SE of 6 mice in each group, ***statistical significant at $p < 0.001$ when compared to the radiation group.

enzymes in mince on exposure to 6Gy whole body irradiation

3.5. Evaluation of anti-inflammatory activity of bark extracts induced during radiation

3.5.1. Estimation of malondialdehyde

M*alondialdehyde* a reactive aldehyde caused by toxic stress in cells and forms a covalent protein adduct. The inflammatory effect caused on radiation would result in the accumulation of the m*alondialdehyde* (Chi et al., 2012). Due to its high cytotoxicity and inhibitory action on protective enzymes, it has been suggested that MDA itself acts as a tumor promoter and a co-carcinogenic agent. Exposure of animals to EB radiation dramatically increased malondialdehyde level in the irradiated mice (5.55 ± 0.11 nmol/mg) group when compared to control group (0.82 ± 0.09 nmol/mg) as represented in (Fig. 4). Hence Pre-treatments with different dose of extracts significantly decreased the malondialdehyde level; comparatively 400mg treated groups showed maximum activity. Similar observations of elevated MDA levels have been reported in rats with gamma radiation. In other related study carried out by Fatih et al. the gamma radiation at 720 cGy elevated the MDA levels in Wistar rats but the treatment of melatonin at 400 mg/g body weight subsequently depleted its level showings it anti-inflammatory activity (Fatih et al., 2004).

3.5.2. Estimation of nitric oxide

Inhibition of nitric oxide by bark extracts of *M. indica* proved anti-inflammatory activity of extracts (Fig. 5). explains nitric oxide estimation in the mice liver exposed to EB radiation (6Gy). The nitric oxide levels were increased in irradiated mice 12.78 ± 1.14 µmol/g when compared to control 2.74 ± 0.14 µmol/g. An administration of M. Indica aqueous stem bark extract orally prior to irradiation at a dose of 400mg (6.756 ± 0.25 µmol/g) reduced nitric acid production when compared to other concentrations i.e. 100mg (8.61 ± 0.31 µmol/g) and 200mg (8.05 ± 0.35 µmol/g). The results suggest that there was increase in nitric oxide concentration in irradiated sample due to increase in nitrate concentrations generated by nitric oxide syntheses by reacting with radical oxygen. Leach et al, 2002. showed that ionizing radiation at low doses activated Ca2+ dependent NOS, while Kim et al, 2013. have shown the up-regulation of nitric oxide synthase in a wide range of tumor cells and tissues during post IR exposure.

3.5.3. Estimation of sialic acid

The serum sialic acid concentrations rapidly increase following the onset of inflammatory disease or injury due to elevated release of globulins in the first inflammatory reaction. Serum sialic acid concentration significantly increased in irradiated mice on EB radiation. So treatment with extracts at 100mg, 200mg and 400mg concentration shows significant reduction in the levels of sialic acid. From (Fig. 6) it can be explained that the *M. indica* (11.12 ± 0.47 µg/ml) extract at 400mg reduced the production of sialic acid levels more significantly ($p > 0.05$) followed by 200mg (11.74 ± 0.04 µg/ml) and 100mg (12.51 ± 0.82 µg/ml). Significant increase in the serum sialic acid levels was observed in mice irradiated parallel to inflammation. The increase in levels of sialic acid might be considered as a defense molecule against the increased oxidative stress. Antioxidant property of sialic acid as a H2O2 scavenger has been reported by (Tanaka et al., 1997) It is well documented that serum sialic acid concentrations rapidly increase following the onset of inflammatory disease or injury. This result suggests that increase in sialic acid during irradiation is due to elevated release of globulins in the first inflammatory reaction (Guo et al., 2012). There by suppression of activity of sialic acid by *M. indica* extracts at 400 mg/kg body weight inhibited the release of globulins thus exhibiting anti-inflammatory activity. Therefore, measure of increase in serum sialic acid concentrations may be a good indicator of inflammatory process.

3.5.4. Histopathology of skin and liver

Histopathology of liver (Fig. 7), showed highly swollen hepatocytes with cytoplasmic vacuolations and apoptosis of hepatocytes in irradiate mice (Fig. 7 (I) B), when compared to normal mice (Fig. 7 (I) A). Also increase in the number of dead cells, inflammatory cells was observed in

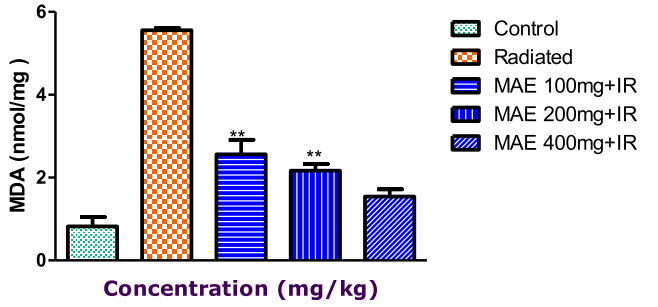

Fig. 4. Effects of *M. indica* on MDA activity in liver after whole body electron beam irradiation. Values are means ± SE of 6 mice in each group, ***statistical significant at $p < 0.001$ when compared to the radiation group.

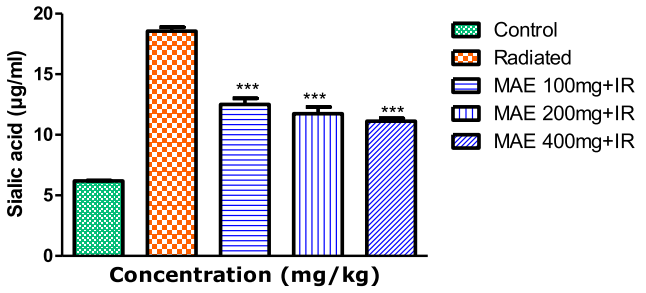

Fig. 6. Effects of *M. indica* on sialic acid activity in liver after whole body electron beam irradiation. Values are means ± SE of 6 mice in each group, ***statistical significant at $p < 0.001$ when compared to the radiation group.

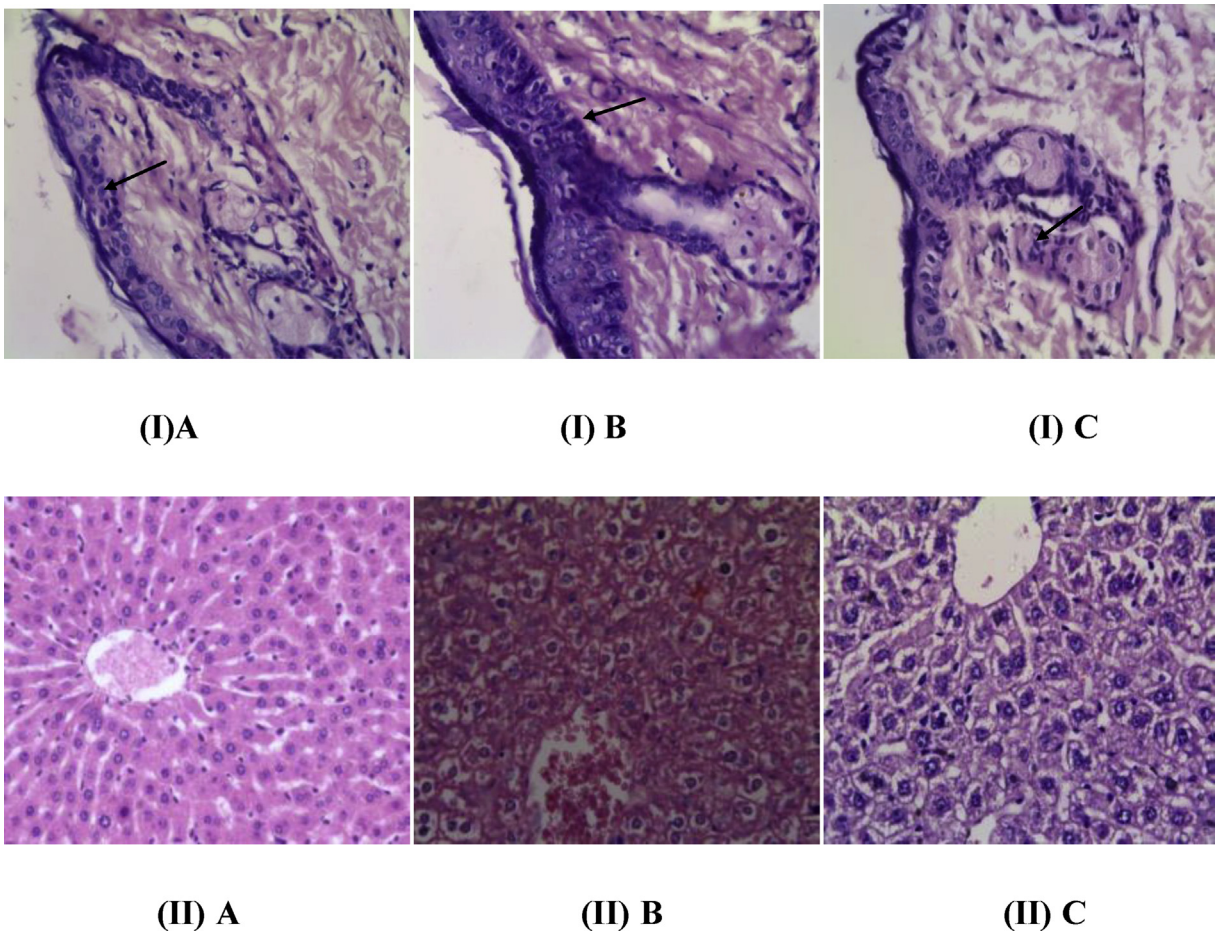

Fig. 7. (I): Histopathology of skin. A: Normal control. B: Irradiated. C: Pretreated with 400 mg/kg M. Indica; 7 (II): Histopathology of liver: A: Normal control. B: Irradiated. C: Pretreated with 400 mg/kg M. *Indica*.

irradiated mice compared to normal. Pretreatment with *M. indica* protected the swollen hepatocytes, apoptosis of hepatocytes, and decreased number of dead and inflammatory cells (Fig. 7 (I) C). Histopathology of skin in irradiated mice (Fig. 7 (II) B) showed apoptosis of epithelial cells in epidermis, condensations of cytoplasm with pyknotic nuclei and also increases in the number of dead cells and NF-kappa cells, when compared to normal mice (Fig. 7(II) A). Treatment with *M. indica* suppressed apoptosis of epithelial cells, and decreased the number of dead and inflammatory cells (Fig. 7 (II) C). Inflammation to skin due to radiation can result in epithelial cell death via apoptosis(Mahil et al., 2006; Scheomaker et al., 2004). Death of these cells is ubiquitous in inflammatory diseases(Hitoshi et al., 2002). On irradiation there was over production of keratin due to hyperkeratosis and death of epithelial cells with pyknotic nuclear formation when compared to control.

3.6. *In silico evaluation*

3.6.1. *Protein-protein interaction network*

To understand the system-level dynamics of a living organism, information about protein cellular pathways and its function is needed. PPI network analysis indicated that PCNA, p53, Mre11, GADD45, BRCA1 and RB1 were found to be hub proteins, which formed numerous interactions with several other proteins involved in the DNA damage process. The merged interacting networks of all 92 proteins obtained from Cytoscape showed the existence of an intra-interaction connection between the partners (interacting proteins of the proteins). The obtained merged network seemed to be connected with 512 nodes and 3163 edges (interactions) between them and is represented in Fig. 8a. Hub nodes obtained from the Cytohubba are represented in Table S5. To reduce the complexity of understanding the network, child network for PCNA from the parent network was retrieved (Fig. 8d) and the interacting proteins with the PCNA were tabulated [Table S6]. Hub proteins in the interacting network are important since it is having the highest number of cliques and also topologically central (Fig. 8c). In the network, nodes are considered as reactions and the metabolites mediated by the influence of nodes are said to be edges. The study of the connection between the proteins provides an enormous insight into robustness and modularity of a given system. PCNA was identified as the hub node in the targeted network (Fig. 8b). This node is found to participate in several pathways involved in the DNA replication, DNA damage and repair pathways. PCNA as a hub mainly interacted with Trp53, Mre11a, Bcl2, Brca1, E2f1, Rb1, Gadd45g and Rad52 as represented in the child network. PCNA interacts with its neighboring proteins to repair the DNA damage aftermath induce by radiation either UV or X-ray etc (Celis et al., 1987). For many proteins that participate in the DNA repair and replication, PCNA acts as a hub node that serves as a docking site, in addition, it increases the efficiency of DNA synthesis. The process of DNA repair is known to begin in a PCNA-p53 mediated manner.

The PCNA-p53 mediated repair process is explained as follows, DNA damage sequentially activates ataxia telengactasia mutated (ATM) and cyclin dependent kinases (Chk2), which phosphorylate substrate protein p53 at various domain sites (S6,S15,S20,W23, L24 etc) and activates -p53 protein. Activated p53, then binds to the promoter region of the PCNA (-236bp to -217bp, p53 binding site) and transactivate the PCNA for DNA repair and processing (Chernov et al., 1998). Brca1 is another protein efficiently recruited to sites of damage; it helps to recruit the PCNA to the

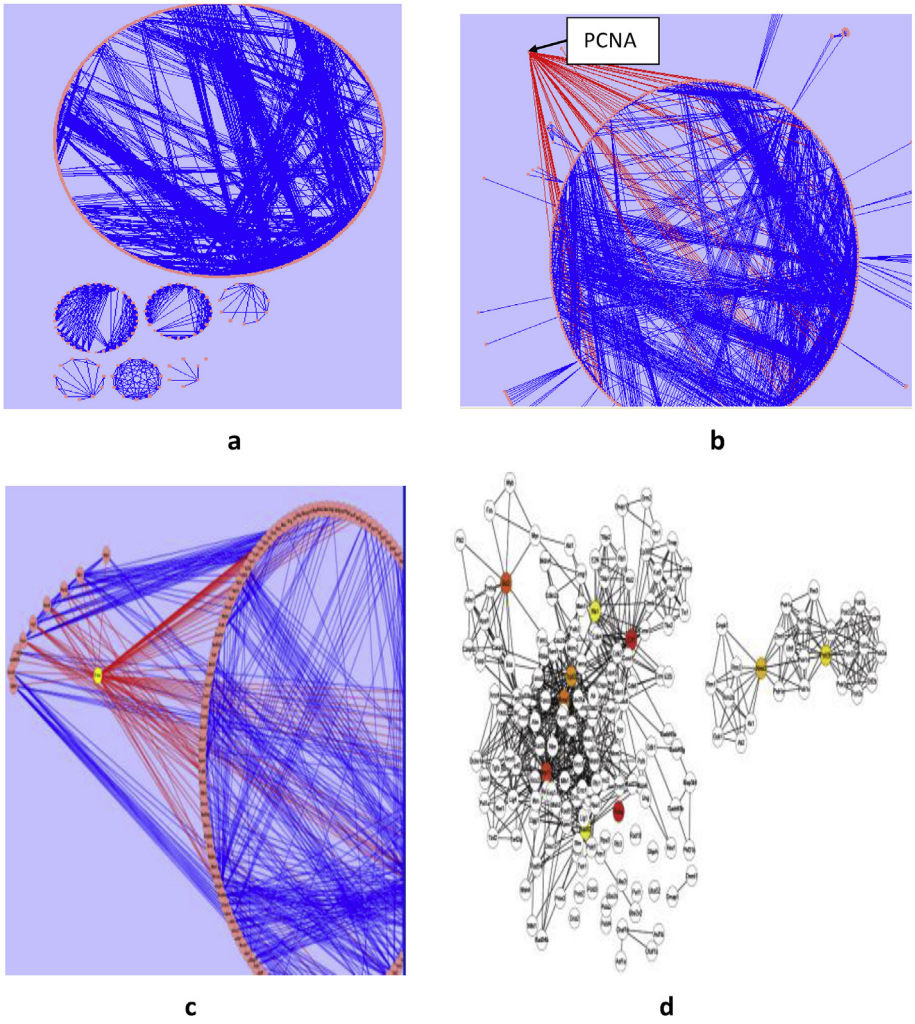

Fig. 8. Merged networks with 512 nodes (proteins), connected with 3163 edges (interactions) between them. a. Overview of the network; b. Interacting network with PCNA as a hub; c. Partners of PCNA; d. 10 ranked hub nodes represented with different colors.

site of DNA damage in cells that are actively replicating their DNA, implying the recruitment process (Nagaraju and Scully, 2007). Simultaneously, DNA binding domain of p53 binds to p53 binding site of growth arrest and DNA damage induced gene (GADD45a) promoter, thereby arresting the cell cycle and delaying cell-cycle progression. PCNA in complex with Brca1, GADD45a and Mre11 then slides on the damaged part of the DNA by recruiting ribonucleotide reductase (p53R2) subunit, which is necessary for the addition of nucleotide at the damaged part of DNA for normal DNA repair process (Maser et al., 1997; Mirzoeva and Petrini, 2001; Chen et al., 1995). But on severe damage to DNA of normal cells, p53 over expressing undergoing apoptosis, this in turn leads to radiation damage (Kastan et al., 1992). Hence inhibition of the function of wild-type p53 in normal tissues suppresses induction of apoptosis and may prevent radiation exposure-associated damage to healthy tissues. This was supported by (Sohn et al., 2009) who suppressed p53 protein using Pifithrin-alpha (PFT-alpha) thereby preventing the severe side effects associated with chemo-and radiotherapy. When switching to cancerous cells, on radiation p53 protein gets mutated in more than 50% of all human carcinomas. Mutated p53 protein, induced by radiation leads to a conformational change, in many cases causing loss of its function and this can lead to the development of radio- and drug-resistant cancer cells. So in another way, activating mutated p53 helps to radio-sensitize the cancerous cells to radiation treatment. A novel concept is specifically targeting tumor suppressor p53 as a key player of apoptosis, to reach radio-sensitization of tumors and radioprotection of normal tissues.

3.6.2. *Validation*

Examining the shortest paths of the above network showed that, two randomly selected nodes of the network connected via 7.753 links to a shared neighborhood distribution with R-squared value of 0.874 and with a correlation value 0.933 with fitted power law of form $y = ax^b$. These results inferring that nodes were closely linked each other and this observation represented in the form of a histogram in Fig. 9a. The cumulative distribution plot shows the clear evidence that the extended network follows scale-free distribution. By measuring the plot drawn on the basis of log transformed cumulative data, α value of 1.140 in the power law distribution was determined (Fig. 9b).

One of the important properties of the network, which follows the scale free distribution, is the existence of a small number of highly connected nodes; called hub, which is more important than other less connected node and which also, acts as a target protein (Kyu and Han, 2009). These target proteins which are known as the hub, which play a crucial role during the survival of the cell and host infection. Other important nodes also have a large BC value. The nodes having top 10° and BC value are shown in Table S7. The network centrality i.e., BC and CC values (Fig. 9 c-d) of the hub protein shows correction value and R square value of 0.980, 0.794 and 0.366, 0.195 respectively. The node having the high BC value was identified as PCNA.

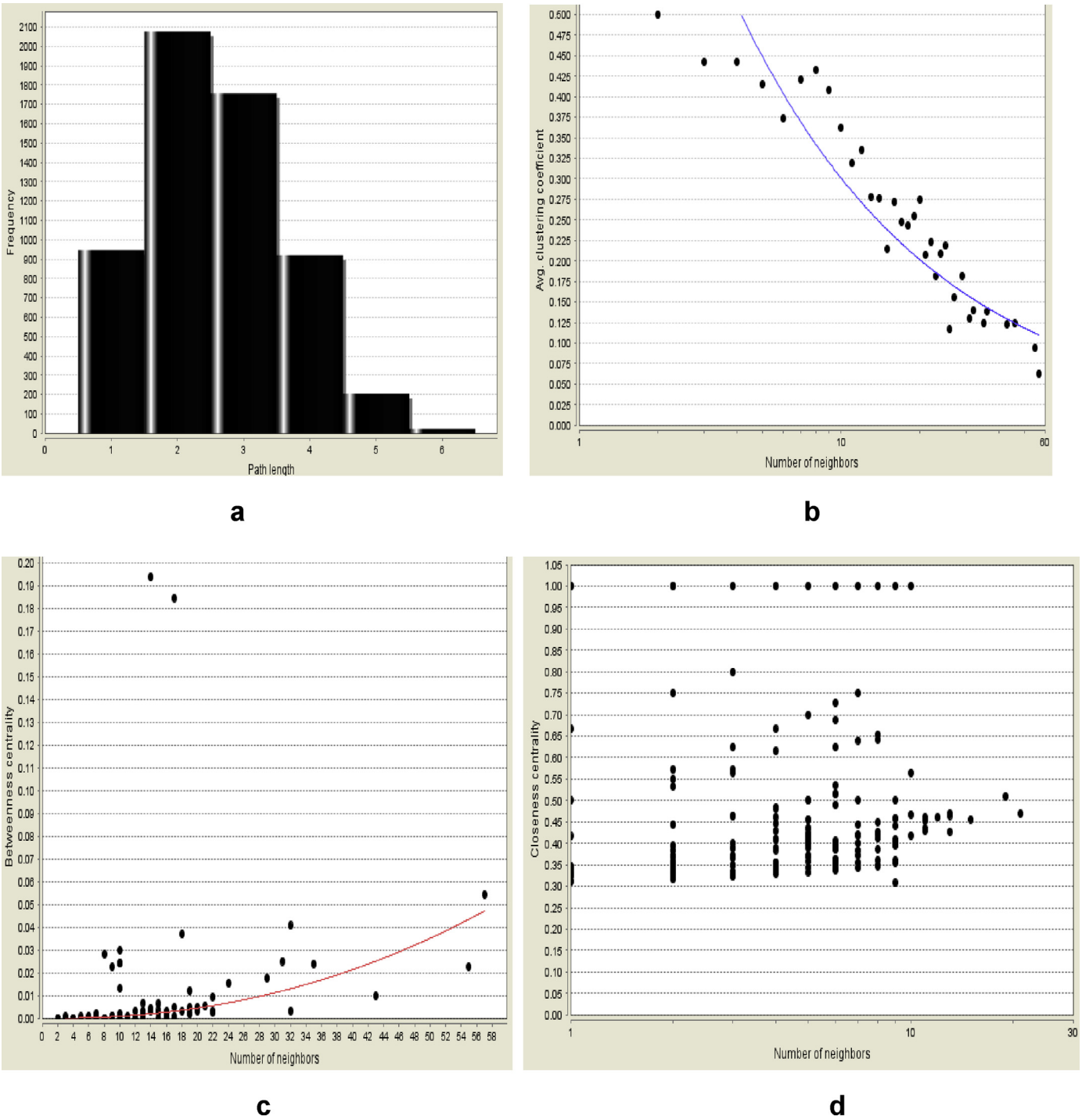

Fig. 9. (a) Histogram showing the distribution of shortest path connected (b) Graphical representation of average clustering coefficient (c) betweenness centrality and (d) closeness centrality of protein-protein interaction.

3.7. QSAR

The actual and predicted values of the compounds along with residual error are represented in Table S8. The graphical representation of actual versus predicted values reveals that the compounds were placed linearly through the axis, indicating that they are structurally related to each other (Fig. 10 a). By statistical analysis, it can be deduced that the structures were correlated with 94% accuracy. The best model was chosen based on statistical values [Table S9]. The model validated by LOF method showed a cross-validated correlation coefficient (q^2) value of 0.937 and a good predictive value (adj r^2, external validation) of 0.937 respectively. In this QSAR model, 94.5% of variance in biological activity was predicted, as indicated by the value of r^2. The QSAR model equation revealed the relationship between the experimental activity as dependent variable and chemical descriptors as independent. Thus, in the present study, the QSAR experiment successfully developed a genetic function approximation (GFA) mathematical model for drug activity prediction.

3.7.1. ADMET

Predicting ADMET properties play an important role in the drug discovery process, because this aims at finding out the behavior of compounds in the whole body by assembling all kinetic properties (Sohn

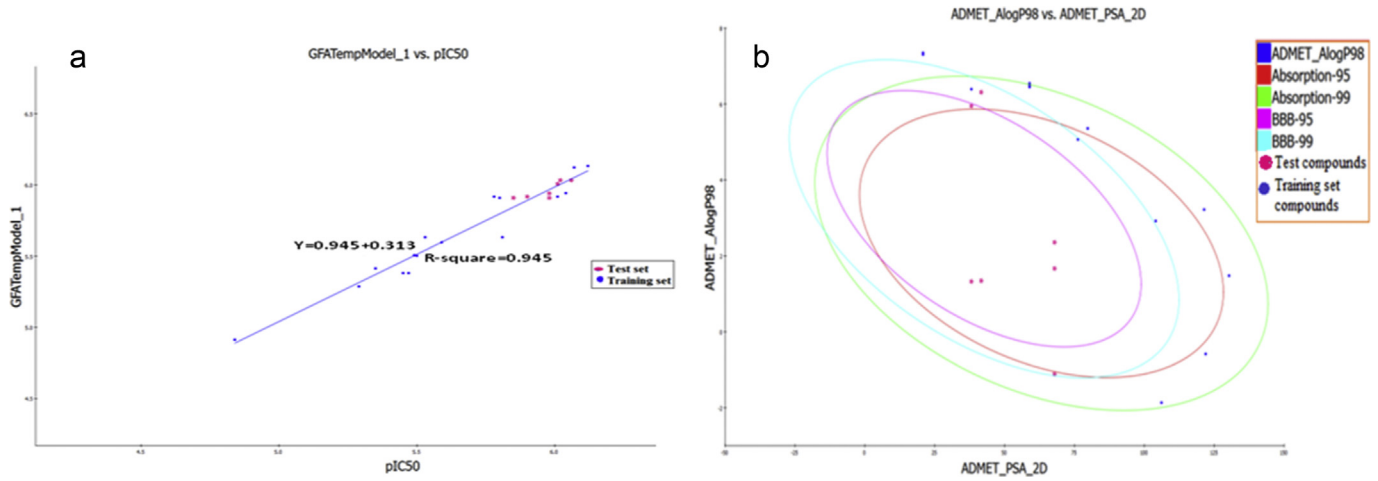

Fig. 10. (a) Activity values predicted by GFA model of test (pink dots) and training (blue dots) set of *M. indica* compounds. (b) ADME properties of compounds of *M. indica*.

et al., 2009). ADMET is applied at an early phase of the drug development process in order to remove the molecules with poor ADMET properties. Pharmacokinetics and pharmacodynamics properties predicted in this study were represented in Table S10. The interpretation of the values was done using standards provided by Accelrys Inc (Ekins et al., 2000). From the table, it can be deduced that the compounds such as quercetin, myricetin, 7-hydroxyflavonol, betulinic acid were proved to have a good ADME profile. The graphical representation of ADMET properties is shown in Fig. 10b.

3.7.2. TOPKAT

TOPKAT studies predicted the aerobic biodegradability, mutagenicity, DTP, skin irritant and carcinogenicity of *M. indica* phytoconstituents [Table S11]. All the compounds showed non-toxic activity except madhusalmone, madhushazone, paltonic acid, betulin and urosilic acid.

3.8. Molecular docking

3.8.1. Binding site prediction of p53 protein

The active pocket residues for p53-DNA binding domain, such as Lys132, Asn239, Ser240, Ser241, Cys242, Asn247, Arg248, Arg249, Pro250, Glu271, Val272, Arg273, Val274, Cys275, Ala276, Asp281 and Glu285, were identified using the interaction energy between the proteins and simple Vander Waals probe to locate the energetically favorable binding sites. It was found that Arg248 and Arg273 were the residues mainly responsible for the binding of p53 to DNA, so blocking these residues from interacting with the DNA gives radioprotection to the normal cells during radiation exposure.

3.8.2. Protein-ligands docking

As summarized in Table S12, the binding conformations and energies of protein-ligand interaction were analyzed by docking studies. The lowest energy conformation represents the best binding conformation of inhibitors to the receptor protein molecule. The complex formed by protein molecule with ligands yielded a plethora of information, highlighting the conclusive role portrayed by numerous factors, namely hydrogen bonds, salt bridges, metal interactions and lipophilic interactions in the protein–ligand interaction profile. A lead molecule is said to be triggered when the binding of drug molecule to the receptor protein is perfectly done. Such an interaction is comparable to the lock-and-key principle, in which the lock encodes the protein and the key is ensemble by the ligand. The major driving force of binding appears to be hydrophobic interaction whose specificity is, however controlled by the hydrogen bonding interactions (Kubinyi, 1998). The docking of phytoconstituents of *M. indica* to p53 protein reveal that the stretch of amino acid residues from Lys132 to Glu285 broadly interact with all the ligands and interestingly coincide with the p53-DNA binding interacting residues i.e. Arg248 and Arg273. The docking scores were obtained from compounds with 1TUP_C as the receptor. The output of all the ligands was given by energy values in kcal/mol as. To determine all possible determinants of the protein, which would probably network with the ligands, non-covalent interactions like hydrogen bonds were analyzed around 5Å distances from the ligand/protein atoms. Amongst all compounds, querciten (docking score 16.62) inhibited p53 protein significantly, which revealed that this compound can serve as a valuable lead molecule to develop novel drugs to inhibit the binding of wild-type p53 to DNA and protect the cells that are exposed to radiation.

4. Conclusion

M. indica aqueous extract exhibited radioprotective activity dose dependently against EB radiation. The radioprotective activity of *M. indica* has proved by protecting DNA from radiation damage in both *in vivo* and *in vitro* models. p53 protein was identified as a hub protein by interacting the proteins involved in the DNA damage process and figured out the underlying mechanism. Molecular docking studies revealed that, querciten exhibited good dock score of -16.62 followed by myricetin and 7-hydroxyflavonol. Examination of binding interactions of the ligands helps in elucidating the reasonable and appropriate structural features of ligand which increase the binding affinity and therapeutic efficacy. Hence, through *in silico* studies, it may be concluded that querciten, myricetin and 7-hydroxyflavonol can be used as novel drugs (radioprotectors) for protecting normal cells from radiation.

Declarations

Author contribution statement

Vinutha K: Performed the experiments; Wrote the paper.

Pavan Gollapalli, Sharath Pattar: Analyzed and interpreted the protein-protein interaction data.

Suchetha Kumari: Contributed reagents, materials, analysis tools or data.

Vidya SM: Conceived and designed the experiments; Wrote the paper.

Funding statement

This work was supported by the Board of Research in Nuclear Science, Government of India (2010/34/04/BRNS/610).

Competing interest statement

The authors declare no conflict of interest.

Additional information

No additional information is available for this paper.

Supplementary content related to this article has been published online at https://doi.org/10.1016/j.heliyon.2019.e01749.

References

Akinmoladun, Ibukun, Afor, Obuotor, Farombi, 2007. Phytochemical constituent and antioxidant activity of extract from the leaves of Ocimum gratissimum. Sci. Res. Essays 2 (5), 163–166.

Barabasi, A.L., Oltvai, Z.N., 2004. Network biology: understanding the cell's functional organization. Nat. Rev. Genet. 5 (2), 101–112.

Berggard, T., Linse, S., James, P., 2007. Methods for the detection and analysis of protein-protein interactions. Proteomics 7 (16), 2833–2842.

Celis, J., Madsen, P., Celis, A., Nielsen, H.V., Gesser, B., 1987. Cyclin (PCNA, auxiliary protein of DNA polymerase delta) is a central component of the pathway(s) leading to DNA replication and cell division. FEBS Lett. 220, 1–7.

Chakma, C.S., 2011. Pharmacological screening of isolated compound from *Madhuca indica longifolia* seeds gives significant analgesic effect. Int. Res. J. Pharm. 2, 43–45.

Chandra, D., 2001. Analgesic effect of aqueous and alcohol extract of *Madhuca indica longifolia*. Indian J. Pharmacol. 33, 108–111.

Chen, I.T., Smith, M.L., Connor, P.M.O., Fornace, A.J., 1995. Direct interaction of Gadd45 with PCNA and evidence for competitive interaction of Gadd45 and p21Waf1/Cip1 with PCNA. Oncogene 11, 1931–1937.

Chernov, M., Ramana, C.V., Adler, V.V., Stark, G.R., 1998. Stabilization and activation of p53 are regulated independently by different phosphorylation events. Proc. Natl. Acad. Sci. Unit. States Am. 95, 2284–2289.

Chi, R.L., Chun, P.K., Wen, H.P., Yuan, S.C., Shang, C.L., Yu, L.H., 2012. Analgesic andanti-inflammatory activities of methanol extract of *Ficus pumila* in Mice. Evid. Based Complement Altern. Med. 9.

Crow, J.P., Ischiropoulos, H., 1996. Detection and quantitation of nitrotyrosine residues in proteins: *in vivo* marker of peroxynitrite. Methods Enzymol. 269, 185–194.

Dahake, A.P., Chiratan, S., 2010. Antihyperglycemic activity of methanol extract of *Madhuka lonifolia* bark. Diabetol. Croat. 39, 3–8.

Daisy, P., Suveena, S., 2012. Solutions to pharmaceutical issues for anti-cancer drugs by Accord excel. Asian J. Pharmaceut. Clin. Res. 5, 149–158.

Das, B.K., Choudhary, B.K., 2010. Quantitative estimation of changes in biochemical constituents of mahua flower during post harvest storage. J. Food Process. Preserv. 34, 831–844.

Denholm, E.M., Wolber, F.M., 1991. A simple method for the purification of human peripheral blood monocytes. A substitute for Sepracell-MN. J. Immunol. Methods 144, 247–251.

Diestel, R., 2000. Graph theory. Graduate Texts in Mathematics. Springer-Verlag, p. 172.

Durga, D.M., Dibyabhaba, P., Manne, M., Amineni, U., 2010. Implementation of computational methods for designing potential inhibitors against human p38α protein. Nature proceedings. https://doi.org/10.1038/npre.2010.5456.1.

Ekins, S., Waller, C.L., Swaan, P.W., Cruciani, G., Wrighton, S.A., Wikel, J.H., 2000. Progress in predicting human ADME parameters in silico. J. Pharmacol. Toxicol. Methods 44, 251–272.

Fatih, S., Erol, C., Topsakal, M., Faik, O., Metin, K., Nevin, I., 2004. Protective effects of melatonin and vitamin E in brain damage due to gamma radiation. Neurosurg. Rev. 27, 65–69.

Freeman, L.C., 1977. A set of measures of centrality based on betweenness. Sociometry 40, 25–41.

Gade, D.R., Pavan, K.K.N.V., Duganath, N., Raavi, D., Kancharla, A., 2012. ADMET, docking studies & binding energy calculations of some novel ACE - inhibitors for the treatment of diabetic nephropathy. Int. J. Drug Dev. Res. 4 (2), 268–282.

Gavin, A.C., Bosche, M., Krause, R., Grandi, P., Marzioch, M., Bauer, A., 2002. Functional organization of the yeast proteome by systematic analysis of protein complexes. Nature 321, 153-141.

Girvan, M., Newman, M.E.J., 2002. Community structure in social and biological networks. Proc. Natl. Acad. Sci. Unit. States Am. 99 (12), 7821–7826.

Gopinathan, G.N., Cherupally, K.N., 2013. Radioprotective effects of gallic acid in mice. BioMed Res. Int. 1–13.

Gorbounova, V., Khokhlova, S., Orel, N., 2000. Docetaxel and cisplatin as first-line chemotherapy in patients with advanced ovarian cancer. Proc Am Soc Clin Oncol 20, 1536.

Grover, S.B., Kumar, J., 2002. A review of the current concepts of radiation measurement and its biological effects. Indian J. Radiol. Imaging 12, 21–32.

Guo, Z., Zhou, B., Li, W., Sun, X., Luo, D., 2012. Hydrogen-rich saline protects against ultraviolet B radiation injury in rats. Journal of Biomedical Research 26.

Hitoshi, A., Jeanne, K., Marie, T.D., Maya, K., Francoise, H., Dominique, K., Fumio, K., Jean, F.N., 2002. Skin inflammation during contact hypersensitivity is mediated by early recruitment of CD8 T-cytotoxic 1 cells inducing keratinocytes apoptosis. J. Immunol. 3079–3087.

Hormozdiari, F., Raheleh, S., Vineet, B.S., Cenk, S., 2010. Protein-Protein interaction network evaluation for identifying potential drug targets. J. Comput. Biol. 17 (5), 669–684.

Jagetia, G.C., Baliga, M.S., Venkatesh, P., Ulloor, J.N., 2003. Influence of ginger rhizome (*Zingiber officinale* Rosc) on survival, glutathione and lipid peroxidation in mice after whole-body exposure to gamma radiation. Radiat. Res. 160, 584–592.

Jindal, A., Soyal, D., Sharma, A., Goyal, P.K., 2009. Protective effect of an extract of *Emblica officinalis* against radiation-induced damage in mice. Integr. Cancer Ther. 8, 98–105.

Kastan, M.B., Zhan, Q., El-Deiry, W.S., Carrier, F., Jacks, T., Walsh, B.S.P., Vogelstein, B., Fornace, A.J., 1992. A mammalian cell cycle checkpoint pathway utilizing p53 and GADD45 is defective in ataxiatelangiectasia. Cell 71, 587–597.

Kim, R.K., Suh, Y., Cui, Y.H., Hwang, E., Lim, E.J., Yoo, K.C., 2013. Fractionated radiation-induced nitric oxide promotes expansion of glioma stem-like cells. Cancer Sci. 104, 1172–1177.

Kubinyi, H., 1998. Structure-based design of enzyme inhibitors and receptor ligands. Curr. Opin. Drug Discov. Dev 1, 4–15.

Kumar, K.B., Kuttan, Ramadasan, 2004. Protective effect of an extract of phyllanthus amarus against radiation-induced damage in mice. J. Radiat. Res. 45 (1), 33–139.

Kyu, K.K., Han, B.K., 2009. Protein interaction network related to Helicobacter pylori infection response. J. Gastroenterol. 15 (36), 4518–4728.

Leach, J.K., Black, S.M., Schmidt-URK, Mikkelsen, R.B., 2002. Activation of constitutive nitric-oxide synthase activity is an early signaling event induced by ionizing radiation. J. Biol. Chem. 277, 15400–15406.

Madhu, L.N., Suchetha, K.N., Vijay, R., 2012. Validation of DNA damage progression with days after single exposure of sublethal dosage of electron beam radiation. J. Appl. Pharm. Sci. 2 (12), 023–026.

Malhi, H., Gores, G.J., Lemasters, J.J., 2006. Apoptosis and necrosis in the liver: A tale of two deaths. Hepatology 43, 31–44.

Maser, R.S., Monsen, J., Nelms, B.E., Petrini, J.H.J., 1997. Mre11and hRad50 nuclear foci are induced during the normal cellular response to DNA double-strand breaks. Mol. Cell. Biol. 17, 6087–6096.

Mirzoeva, O., Petrini, J.H.J., 2001. DNA damage dependent nuclear dynamics of the MRE11 complex. Mol. Cell. Biol. 21, 281–288.

Nagaraju, G., Scully, R., 2007. Minding the gap: the underground functions of BRCA1 and BRCA2 at stalled replication forks. DNA Repair 6, 1018–1031.

Nair, S.R., Subhashini, R., Thiagarajan, B., 2010. Comparative docking analysis on natural compounds versus a synthetic drug as a therapeutic for acquired immuno deficiency syndrome. Am. Med. J. 1, 148-150.

Newman, M.E.J., Girvan, M., 2005. Finding and evaluating community structure in networks. Soc. Netw. 27, 39–54.

Nitin, M.G., Cherupally, K.N., 2004. Radiation protection by diethyldithicarbamate: protection of membrane and DNA *in vitro* and *in vivo* against γ-radiation. J. Radiat. Res. 45 (2), 175–180.

Ohkawa, H., Odisha, N., Yagi, K., 1979. Assay for lipid peroxides in animal tissues by thiobarbituric acid reaction. Anal. Biochem. 95, 351–358.

Pawar, R.S., Bhutani, K.K., Madhucoside, A., 2004. Protobassic acid glycosides from Madhuca indica with inhibitory activity on free radical release from phagocyte. J. Nat. Prod. 67 (4), 668–671.

Pearl, A.D., Lathika, S., Suchetha, K.N., 2014. Safety evaluation of a herbal mixture of aqueous extracts of *Ficus racemosa* and *Azadirachta indica*: assessment of sub-chronic toxicity in rats. World J. Pharmaceut. Res. 3 (10), 1019–1026.

Pedamallu, C.S., Posfai, J., 2010. Open source tool for prediction of genome wide protein-protein interaction network based on ortholog information. Source Code Biol. Med. 5.

Rogers, D., Hopfinger, A.J., 1994. Application of genetic function approximation to quantitative structure activity relationship and quantitative structure-property relationship. J. Chem. Inf. Comput. Sci. 24, 854.

Sancar, A., Lindsey-Boltz, L.A., Unsal-Kaçmaz, K., Linn, S., 2004. Molecular mechanisms of mammalian DNA repair and the DNA damage checkpoints. Annu. Rev. Biochem. 73, 39–85.

Sankar, A.M., Shanmughavel, P., 2010. In silico docking analysis for viral protein hemagglutinin neuraminidase against the synthetic drugs for human parainfluenza virus 2. Int. J. Pharma Bio Sci. 2, 1–12.

Schoemaker, M.H., Moshage, H., 2004. Defying death: The hepatocyte's survival kit. Clin. Sci. 107, 13–25.

Shannon, P., Markiel, A., Ozier, O., 2002. Cytoscape: a software environment for integrated models of bio-molecular interaction networks. Genome Res. 12 (11), 2498–2504.

Shu-Hwa, C., Chia-Hao, C., Hsin-Hung, W., Cyto-Hubba, 2010. Identifying hub objects and sub-networks from complex interactome. BMC Syst. Biol. 8 (4), 11.

Singh, N.P., 2000. Microgel for estimation of DNA strand breaks, DNA protein crosslink's and apoptosis. Mutat. Res. 455, 111–127.

Sohn, D., Graupner, V., Neise, D., Essmann, F., Schulze-Osthoff, K., Jänicke, R.U., 2009. Pifithrin-alpha protects against DNA damage induced apoptosis downstream of mitochondria independent of p53. Cell Death Differ. 16, 869–878.

Suel, B., Lehmann, G., Bork, P., Huynen, M.A., 2000. STRING: a web-server to retrieve and display the repeatedly occurring neighborhood of a gene. Nucleic Acids Res. 28 (18), 2442–2444.

Szumiel, I., 2006. Epidermal growth factor receptor and DNA double strand break repair: the cell's self-defence. Cell. Signal. 18 (10), 1537–1548.

Tanaka, K., Tokumaru, S., Kojo, S., 1997. Possible involvement of radical reactions in desialylation of LDL. FEBS Lett. 413, 202–224.

Vedansha, J., Pragati, M., Shukla, P.K., Ramteke, P.W., Tiku, A.B., 2012. In vitro DNA damage characterisation studies on plasmid pBR322 after exposure to γ radiation by ^{60} Co. J. Radioanal. Nucl. Chem. 291 (3), 661–664.

von Mering, C., Krause, R., Snel, B., 2002. Comparative assessment of large-scale data sets of protein-protein interactions. Nature 417 (6887), 399–403.

Warren, J., 1959. Unidentified curved bacilli on gastric epithelium in active chronic gastritis. Lancet 1273.

Watts, D.J., Strogatz, S.H., 1998. Collective dynamics of small world networks. Nature 292 (6684), 440–442.

Yang, L., Xu, L., He, L.A., 2009. CitationRank algorithm inheriting Google technology designed to highlight genes responsible for serious adverse drug reaction. Bioinformatics 25, 2244–2250.